ELSEVIER

Journal of Structural Geology 28 (2006) 1685–1693

JOURNAL OF STRUCTURAL GEOLOGY

www.elsevier.com/locate/jsg

Displacement accumulation from earthquakes on isolated normal faults

T. Manzocchi [a,*], J.J. Walsh [a], A. Nicol [a,b]

[a] *Fault Analysis Group, School of Geological Sciences, University College Dublin, Belfield, Dublin 4, Ireland*
[b] *GNS Science, Lower Hutt, New Zealand*

Received 26 October 2005; received in revised form 8 June 2006; accepted 20 June 2006
Available online 21 August 2006

Abstract

Displacement profiles for isolated normal faults are most often triangular rather than semi-elliptical as predicted for linear elastic materials. Simple modelling indicates that triangular displacement profiles can arise from Gutenberg–Richter earthquakes randomly distributed on fault surfaces of constant dimensions. Near-triangular profiles are generated after a small number of earthquake cycles and for earthquake magnitude ranges as small as 0.5. The results are only weakly dependent on the shape of earthquake slip profiles, and reproduce the geometry of displacement profiles on the non-propagating active Cape Egmont Fault in New Zealand. By contrast, growth models in which fault displacement and length increase in proportion result in unrealistic displacement profiles for realistic slip profiles irrespective of whether earthquake populations are Characteristic or Gutenberg–Richter.

Keywords: Faults; Fault growth; Fault displacement; Characteristic earthquakes; Gutenberg–Richter

1. Introduction

Earthquake slip events are ideally characterised by the semi-elliptical slip profiles expected for ruptures within linear elastic materials (Eshelby, 1957; Pollard and Segall, 1987). It is now generally accepted, however, that these slip profiles combine to provide long-term displacement profiles that are most often triangular in shape, with departures from triangular displacement profiles generally attributed to strong interactions with adjacent faults or to rheological effects (Nicol et al., 1996; Manighetti et al., 2001). A variety of fault growth models have been advanced to explain both the triangular shape of displacement profiles and the well-established displacement/length scaling on faults (Walsh and Watterson, 1987; Cowie and Scholz, 1992; Manighetti et al., 2004). A feature of all such models is that each slip event ruptures the entire fault surface, providing Characteristic earthquakes (Schwartz and Coppersmith, 1984), and is responsible for fault propagation. The predicted propagation is independent of whether elastic strains are relaxed between each slip increment (Walsh and Watterson, 1987), permitted to accrue on the fault (Cowie and Scholz, 1992) or partially relieved by minor faulting in a damage zone (Manighetti et al., 2004). A growing body of evidence suggests, however, that fault propagation is a feature principally of the earliest phase of fault activity and that normal faults often accumulate displacement whilst maintaining near constant lengths for the majority of their growth history (Morewood and Roberts, 1999; Poulimenos, 2000; Meyer et al., 2002; Walsh et al., 2002; Childs et al., 2003; Nicol et al., 2005). In these circumstances, triangular profiles can only be produced by relaxing the requirements for Characteristic earthquakes or by abandoning the notion of semi-elliptical slip profiles.

In this paper we reproduce the triangular displacement profiles that are typical of non-interacting faults using a simple stochastic model in which a Gutenberg–Richter (G–R) (i.e. power-law; Gutenberg and Richter, 1944) population of earthquakes occurs on a fault surface of fixed dimensions. The placement of earthquakes on the fault is assumed to be entirely random on the basis that (i) associated elastic strains are

* Corresponding author. Tel.: +353 1 7162605; fax: +353 1 7162607.
E-mail address: tom@fag.ucd.ie (T. Manzocchi).

0191-8141/$ - see front matter © 2006 Elsevier Ltd. All rights reserved.
doi:10.1016/j.jsg.2006.06.006

relaxed on geological time scales (e.g. thousands to millions of years) and (ii) the spatio-temporal correlations of earthquake behaviour on isolated faults is a short-term phenomenon, occurring on time scales much less than the several G–R cycles examined in our modelling. Results indicate that even after small numbers of earthquake cycles and very modest (>0.5) ranges in earthquake magnitude, near-triangular profiles are generated irrespective of the shape of earthquake slip profiles.

A comparison of model results with the Cape Egmont Fault from New Zealand's Taranaki Basin, which did not grow in length during much of its most recent period of growth (0–3.7 Ma BP) indicates that it is not possible to infer either the shapes of slip events or the magnitude range of earthquakes from the shape of the displacement profiles – the near-triangular displacement profiles observed on nine horizons could have arisen from a variety of earthquake slip profiles, including elliptical ones, and for different ranges in earthquake magnitudes.

Finally, we re-examine existing inelastic geometrical fault profile evolution models for propagating faults (e.g. Walsh and Watterson, 1988; Gillespie et al., 1992; Peacock and Sanderson, 1996) and include G–R, as well as Characteristic, earthquake populations in the models. Results indicate that elliptical slip distributions can generate near-triangular displacement distributions on propagating faults only if the earthquake population is near-Characteristic and if the displacement/length scaling exponent is higher than generally measured ($n > 1.5$).

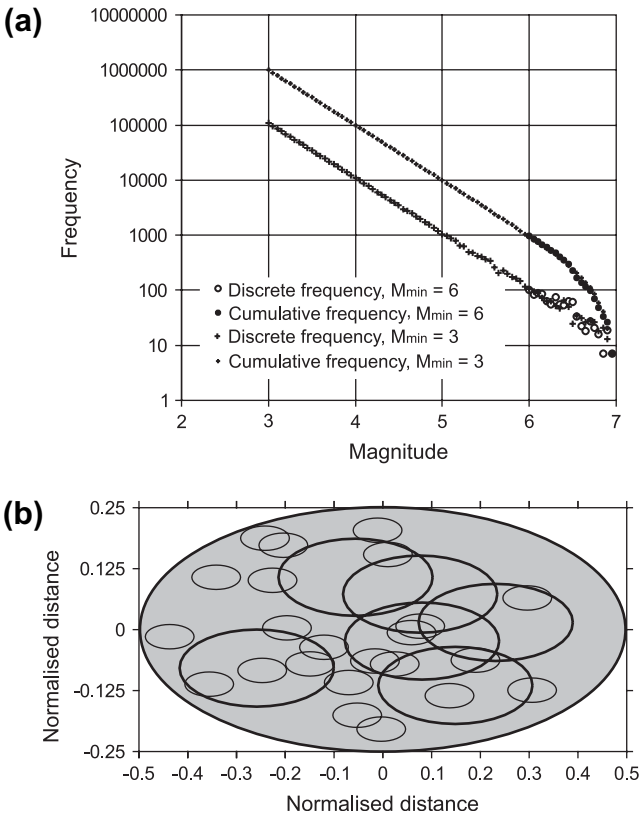

Fig. 1. (a) Magnitude frequency and cumulative frequency of earthquake populations for realisations of 100 G–R cycles covering earthquake magnitude ranges of 4 and 1. (b) Idealised elliptical model fault (grey) showing the rupture areas of six M6 and 20 M5 randomly positioned earthquakes.

2. Displacement profiles for non-propagating faults

A stochastic model of a G–R population of earthquakes is used to simulate normal fault growth by the accumulation of co-seismic slip (Fig. 1). For illustrative purposes, we have chosen to model an elliptical fault surface capable of supporting a maximum earthquake of magnitude 7. G–R populations containing earthquakes of magnitude $7 > M \geq M_{\min}$ are generated for different values of $M_{\min}$ and a range of G–R cycles. Each population defines a power-law magnitude frequency distribution over the modelled range in M, while the cumulative magnitude frequency distribution shows the characteristic roll-off (e.g. Main, 1990) at high M (Fig. 1a). The value of the cumulative frequency population extrapolated to M7 is equivalent to the number of G–R cycles present. Models considered contain up to 10^7 earthquakes, between 0.1 and 100 G–R cycles and with $M_{\min}$ ranging from 2 to 6.9.

The moment (M_0) of an earthquake is related empirically to its magnitude through $\log(M_0) = cM + d$, where $c \approx 1.5$ and $d \approx 9.1$ (e.g. Scholz, 1990), and to the dimensions of the rupture through $M_0 = \mu\langle u\rangle A$, where μ is the shear modulus (taken as 10 GPA, e.g. Walsh and Watterson, 1988), $\langle u\rangle$ is the average co-seismic slip and A is the rupture area. We model elliptical ruptures with principal radii of length $r_1 = 2r_2$ (Fig. 1b). The empirical ratio between maximum co-seismic slip ($u_{\max}$) and rupture length ($2r_1$) of 5×10^{-5} (Wells and Coppersmith, 1994) is used. Each model comprises earthquake ruptures with one of three slip shapes: conical profiles (triangular in 1D) in which $\langle u\rangle = u_{\max}/3$, semi-ellipsoidal profiles (elliptical in 1D) in which $\langle u\rangle = 2u_{\max}/3$, and disc-shaped profiles (rectangular in 1D) in which $\langle u\rangle = u_{\max}$ (Fig. 2). These relationships define the dimensions ($u_{\max}$, r_1) of each model earthquake from its magnitude. For example, a conical M7 model earthquake has a maximum slip of 4.2 m and a maximum rupture length of 85 km, while a disc-shaped one has $u_{\max} = 2.9$ m and $2r_1 = 59$ km. The smallest events considered (M2) have $u_{\max} \approx 1$ cm and $2r_1 \approx 200$ m. The fault surface is scaled by the dimensions of the largest possible earthquake (M7) and individual ruptures are placed randomly on the fault with the single constraint that each rupture must be contained entirely within the fault surface (Fig. 1b).

Models with elliptical slip profiles, $M_{\min} = 4$ and different numbers of G–R cycles are discussed (Figs. 3 and 4) before examining the dependence of the shape of the slip profiles and the range of earthquake sizes on the resultant displacement profiles (Fig. 5). The accumulation of displacement is examined either on the entire fault surface (e.g. Fig. 3a–c) or on 1D sections through the long axis of the fault (Fig. 3d–f). Profiles on any other chord of the fault are broadly similar in shape. Profiles at fractions of a G–R cycle are characterised by high displacement gradients and irregular shapes (Fig. 3a) but as the fault accumulates more earthquakes the shape of the profile becomes gradually more regular (Fig. 3b). An essentially smooth displacement profile emerges

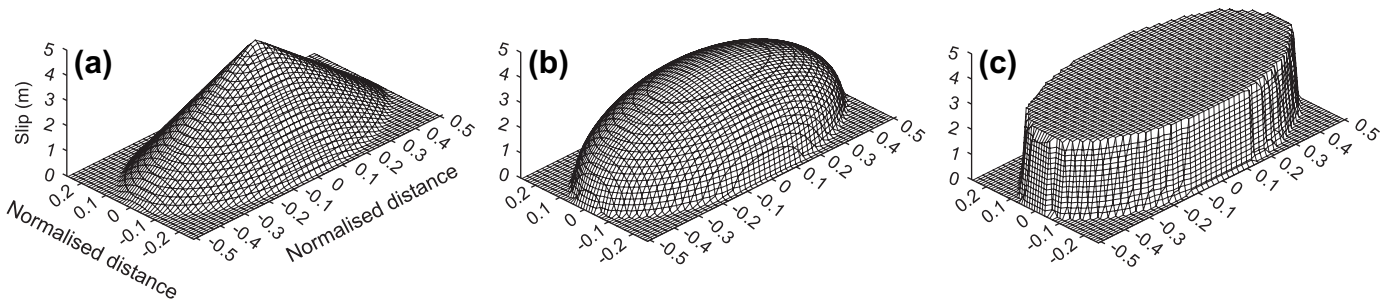

Fig. 2. M7 earthquakes with triangular (a), elliptical (b) and rectangular (c) slip profiles. The moment of each earthquake is the same (3.98×10^{19} N m) and the maximum slips are 4.236 m (a), 3.362 m (b) and 2.937 m (c).

by ca. 10 G–R cycles (Fig. 3c) and, significantly, the displacement profile shape does not mirror the shape of the individual ruptures that formed it (shown for this model in Fig. 2b).

Average characteristics of the displacement profiles and their variability are summarised by examining multiple realisations of the model. The accumulation of displacement per G–R cycle at the centre of the fault (D/N) is, on average, constant irrespective of the number of G–R cycles (Fig. 4a), but is highly variable at small fractions of a cycle. This variability decreases systematically with the number of earthquake cycles (N); for example, the standard deviation of maximum fault displacement per cycle ($\sigma^2_{D/N}$) scales with N through the power-law relationship $\sigma^2_{D/N} \approx 4N^{-0.5}$. Stable displacement profiles ($\sigma^2_{D/N} < 0.5D/N$) are formed after ca. 1 G–R cycle.

A simple factor (Δ) characterising the shape of the profiles in 1D is given by the average displacement of the fault on the profile normalised by the displacement at the fault centre. A triangular displacement profile has $\Delta = 0.5$, an elliptical one $\Delta = 0.75$ and a rectangular one $\Delta = 1.0$. The evolution of the displacement profile shape with the accumulation of G–R cycles is shown in Fig. 4b. The displacement profiles are extremely variable for fractions of a G–R cycle, but a constant average profile shape ($\Delta = 0.6 \pm 0.15$) emerges after one cycle, equivalent to a maximum fault displacement of 10 m for these models in which $M_{max} = 7$. The variability in shape progressively decreases, culminating in a value of $\Delta = 0.6 \pm 0.01$ after 100 G–R cycles. This shape factor is closer to $\Delta = 0.5$, which would be obtained by modelling Characteristic earthquakes with triangular slip profiles, than it is to $\Delta = 0.75$, representative of the displacement profile shape factor resultant from Characteristic earthquakes with the input, elliptical, slip profiles.

This examination (Figs. 3 and 4) of a single system indicates that stable fault profiles emerge from a random placement of power-law earthquake ruptures at low numbers of G–R cycles. A particularly useful geological measure of how rapidly stability arises is provided by the maximum displacement of our model faults, a measure which is independent of the recurrence intervals between cycles. Our modelling shows that stable profiles emerge at maximum displacements of 10 m (1 G–R cycle) and that even for 10 G–R cycles, the maximum displacements are, in geological terms, very modest ($\sim$100 m) – perhaps more surprising, however, is the emergence of semi-triangular displacement profiles from elliptical slip profiles.

The precise form of the displacement profile is a function of both the shapes of the earthquake ruptures and the magnitude range of earthquakes; as discussed above, the number of G–R cycles influences the variability of the expected profile

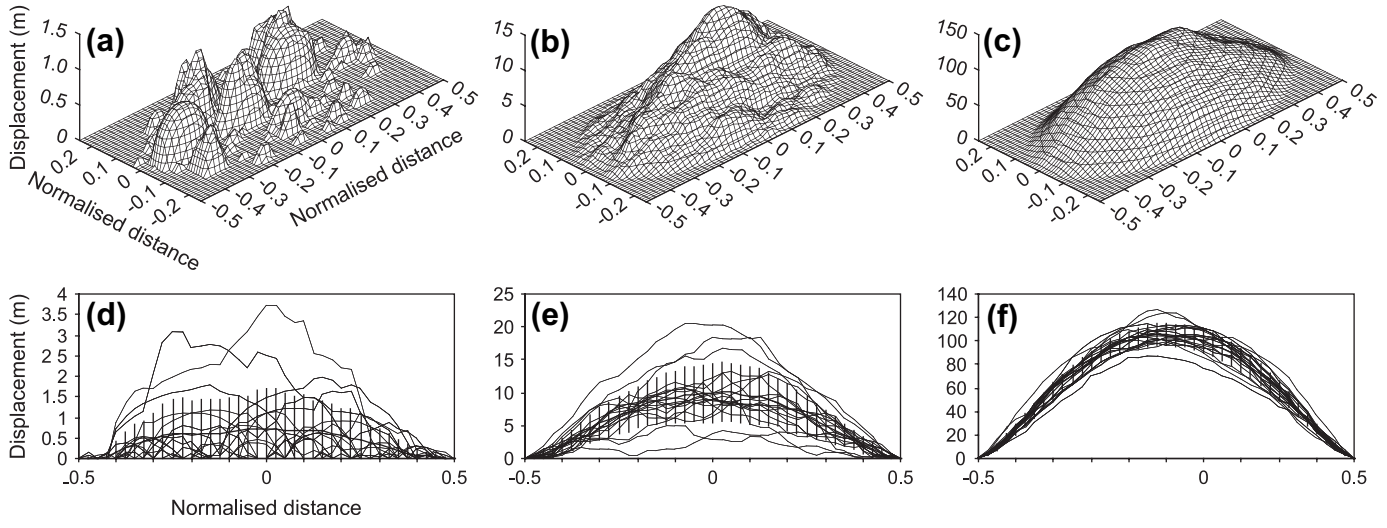

Fig. 3. Displacement on the fault for a model realisation containing earthquakes with elliptical slip profiles in the range M4–M7 after 0.1 (a), 1 (b) and 10 G–R cycles (c). (d)–(f) 1D displacement profiles on the long axis of the fault for 20 realisations of these systems (thin lines), with the mean displacement profile shown as the thicker line. Error bars are ± 1 standard deviation.

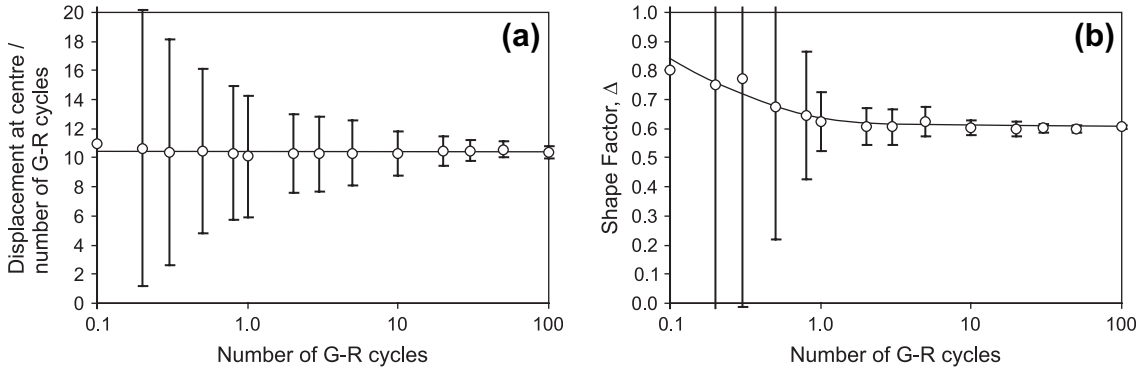

Fig. 4. Evolution of (a) displacement at the fault centre per G–R cycle and (b) shape factor (average displacement/displacement at the centre of the fault) as a function of the number of G–R cycles, for a fault containing earthquakes with elliptical slip profiles in the range M4–M7. Error bars reflect the standard deviation observed from multiple realisations of the system. Stable fault shapes emerge after ca. 1 G–R cycle.

but not its expected shape. Fig. 5 summarises the average profiles obtained from realisations of models containing 10 G–R cycles with different values of M_{min} for the three different rupture shapes. Faults accumulating displacement from strictly Characteristic earthquakes (i.e. $M_{min} = 7$) have shape factors equivalent to the slip profile shape factor, but as the range in magnitude of the earthquakes increases the shape factor of the displacement profile changes, with minimum values of Δ (in the range 0.45 for triangular slip profiles to 0.6 for rectangular ones) occurring at an M-range of ca. 0.8 (Fig. 5d). Once the M-range is greater than 2 (i.e. $M_{min} < 5$), Δ is no longer dependent on M_{min}, converging to $\Delta = 0.52 \pm 0.04$ for triangular slip profiles, 0.6 ± 0.04 for elliptical ones, and 0.66 ± 0.04 for rectangular ones.

The shape factor (Δ) is a first order approximation to the shape of the displacement profiles and does not, for example, discriminate between strictly triangular profiles with constant displacement gradients and bell-shaped profiles with an inflection point which can also have $\Delta = 0.5$ (e.g. for triangular slip profiles with $M_{min} = 6.0$, Fig. 5a). The broad minima in Δ,

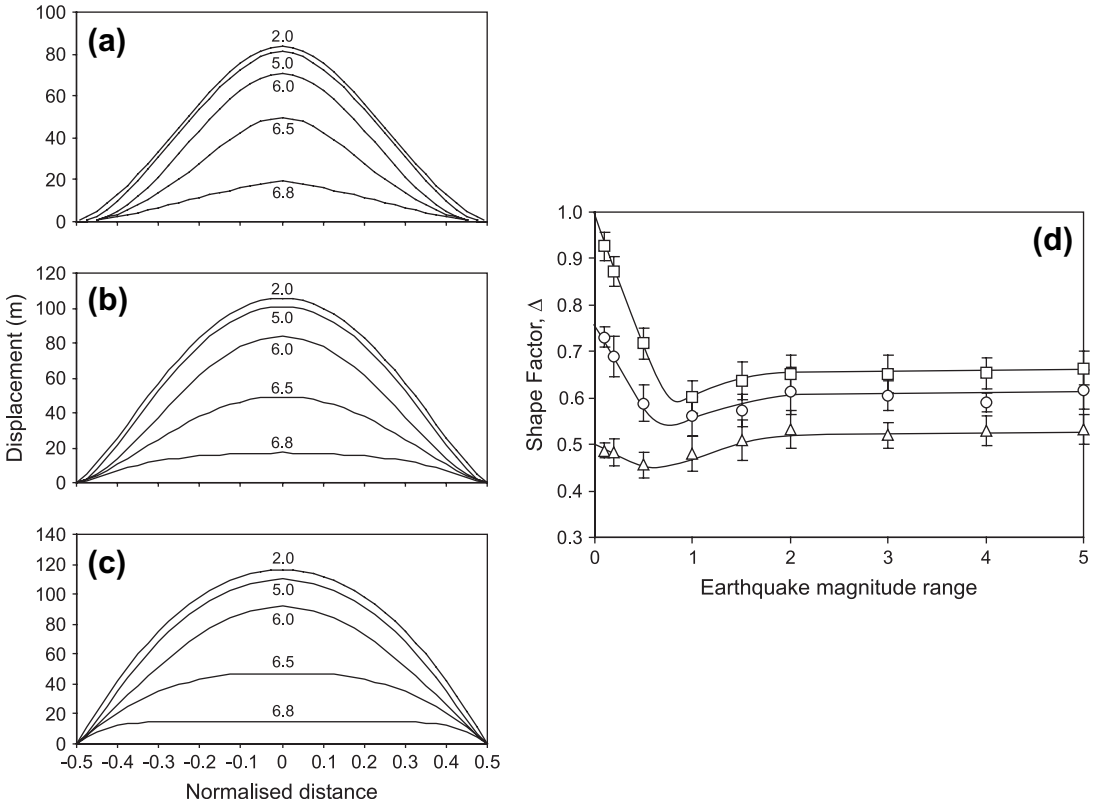

Fig. 5. Average 1D displacement profiles after 10 G–R cycles for earthquakes with triangular (a), elliptical (b) and rectangular (c) slip profiles. Profiles are shown for models with different values of M_{min} (labelled). (d) Fault displacement shape factor vs. the magnitude range of earthquakes for 10 G–R cycles of triangular (triangles), elliptical (circles) and rectangular (squares) slip profiles. Error bars are ± 1 standard deviation.

obtained for each slip profile shape at a magnitude range of ca. 0.8 (Fig. 5d), is a consequence of lower normalised displacement gradients close to the fault tip and an inflection point closer to the centre of the fault with this scale-range of ruptures. Profiles become less bell-shaped as the range in earthquake sizes increases.

3. Comparison to the Cape Egmont Fault

The modelling results are compared to displacement profiles for the Cape Egmont Fault (CEF) in offshore New Zealand (Fig. 6). This normal fault is a reactivated structure with a maximum displacement of about 2500 m that accrued over the last 3.7 Ma (Nicol et al., 2005). The kinematic evolution of the fault during this most recent period of activity has been described in detail by Nicol et al. (2005) who constructed the displacement profiles on nine horizons (the seabed, three of Late Quaternary age and five of Pliocene–Early Pleistocene age) summarised in Fig. 6b. The profiles are approximately triangular ($0.45 < \Delta < 0.6$) and indicate that the fault maintained a ca. 70 km constant fault length, with the point of maximum displacement occurring within the central 15 km of the fault (Fig. 6b). The fault grew by reactivation of a pre-existing late Miocene and Cretaceous structure and upward propagation through a ca. 500 m thick Pliocene cover sequence. Apart from the upward propagation of the fault through overlying syn-rift sediments, the increase in fault surface area in the entire Pliocene–Pleistocene growth

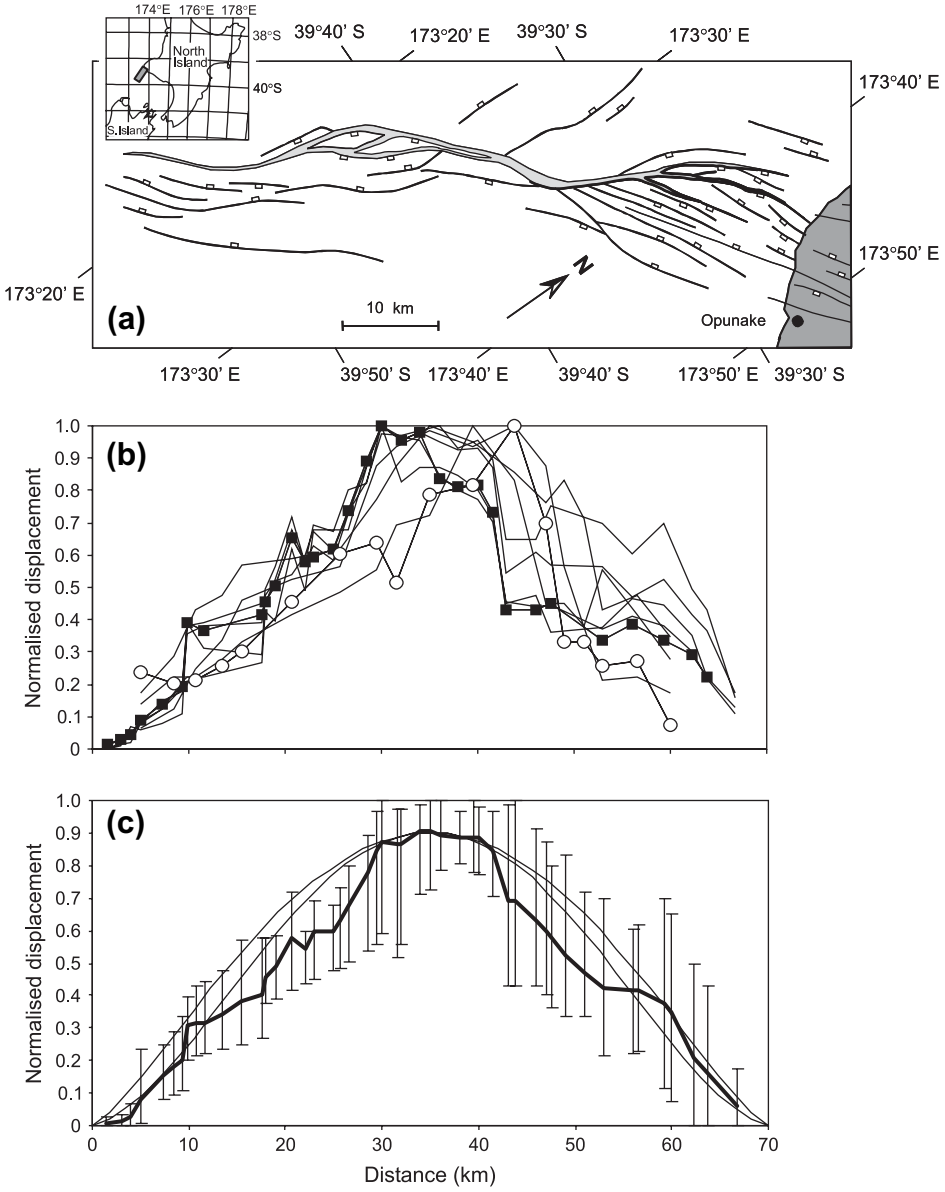

Fig. 6. (a) Location of the Cape Egmont Fault showing fault traces mapped on the 3.7 Ma horizon. (b) Normalised fault displacement profiles for nine horizons ranging in age from ca. 7 ka (seabed, open circles) to ca. 5.3 Ma (squares). (c) Comparison of the normalised profiles with model output for faults likely to rupture the ground surface ($M_{min} = 6$, lower curve) and lower horizons ($M_{min} = 2$, upper curve) assuming elliptical earthquake slip profiles. The thicker line and error bars show the average and range from the individual horizons. The fault displacement data derived from Nicol et al. (2005).

history was only ~2% (Nicol et al., 2005). Although the displacement profiles of different horizons are similar to each other, they represent displacement accumulation over time intervals ranging from ca. 7 ka to 3.7 Ma, corresponding to maximum displacements of 6 m at the seabed to 2.5 km on the oldest horizon. Displacements on the younger horizons (and in particular the seabed) are unlikely to have been produced by earthquakes smaller than magnitude 5.5–6, since rupture of the ground surface is typically produced by earthquakes of this magnitude and above (e.g. McCalpin and Nelson, 1996). The older horizons accumulated displacements throughout their burial to their present depths, and therefore may have been subjected to progressively larger scale-ranges of earthquakes.

The CEF displacement profiles represent displacement accumulation within ca. 4 km of the earth's free surface, on a seismogenic fault which most closely resembles a rectangular, rather than elliptical, shape. Although we have modelled elliptical faults, identical displacement profiles are obtained on a rectangular fault provided, as is the case for the CEF, that the maximum possible earthquake magnitude is limited by the length, rather than width (i.e. in this case, the down-dip dimension) of the fault. A comparison with model displacement profiles generated by G–R earthquakes with elliptical slip profiles and $M_{\min}$ in the range 6.0–2.0 (Fig. 6c) shows that (i) the value of $M_{\min}$ considered does not significantly influence the shape of the resultant normalised displacement profiles (see also Fig. 5b, d) and (ii) the CEF displacement profiles are broadly compatible to these G–R model profiles. As discussed by Nicol et al. (2005), the profiles aggregate displacements on the main fault and on synthetic splays, but do not include contributions from antithetic faults. Antithetic faults account for less than 5% of the total displacement in the central 30 km of the fault and increase in relative significance towards the tips, particularly at the northern end of the fault where they account for up to 30% of the total displacement. The regions where the average measured profiles depart most from the model profiles (i.e. between 15–25 km and 45–55 km; Fig. 6c), therefore, contain the regions in which antithetic faults become more significant, and their omission from the aggregate displacement profiles may contribute in part to the displacement deficits relative to the modelled profiles. These regions also correspond to the two main bends in the fault (Fig. 6a) and hence may be positions where fault displacements have been preferentially converted to ductile strains (bed rotations) accommodating a portion of the cumulative earthquake slip. Therefore, while it is not possible to identify precisely the causes of irregularities in the displacement profiles, they nonetheless have an overall form similar to the modelled profiles.

The short duration of the historical seismicity record associated with the CEF does not permit characterisation of the earthquake population that produced the fault displacements, which could have arisen from Characteristic earthquakes with approximately triangular slip profiles from G–R earthquakes with a range of slip profile shapes. However, only the second possibility reconciles both the observed displacement profiles, and ideal, elliptical, earthquake slip profiles.

4. Displacement profiles for propagating faults

The Cape Egmont Fault has demonstrably accumulated displacement with a near constant length (Nicol et al., 2005), however, the kinematic constraints on fault growth needed to establish a growth history are only rarely available. Fault growth histories in which propagating faults accumulate displacement in (either linear or power-law) proportion to their length have generally been inferred from the geometrical characteristics of different size faults in the same population, rather than from kinematic analysis of individual faults. Since kinematic histories are unavailable for these fault populations, they can neither confirm nor disprove propagation. Therefore, despite the observation that where the necessary kinematic histories are available faults are shown to accumulate displacement without propagation over most of their growth history (Morewood and Roberts, 1999; Poulimenos, 2000; Meyer et al., 2002; Walsh et al., 2002; Childs et al., 2003; Nicol et al., 2005), it remains possible that some faults grow in displacement and length synchronously, along the maximum displacement to length relationship $D = BL^n$ of the fault population. Previous models that assume Characteristic earthquakes on propagating faults have shown that the resultant displacement profiles depend on the power-law exponent n (Gillespie et al., 1992), and, at a particular value of n, on the fault propagation rate (Peacock and Sanderson, 1996).

Despite the lack of supporting kinematic evidence there are no intrinsic problems with the notion that displacement might accumulate along a growth trend $D = BL^n$, through repeated earthquakes of slip $u_{\max} = 5 \times 10^{-5}L$ where $B \gg 5 \times 10^{-5}$, even if $n = 1$. Fault growth with different values of B and n can be modelled using a power-law fault propagation function $\mathrm{d}L = p_1 L^{p_2}$ (e.g. Cladouhos and Marrett, 1996), where $\mathrm{d}L$ is the increase in length of the fault per earthquake, L is the fault length and p_1 and p_2 are constants that can be deduced from B and n. The increase in maximum fault displacement per earthquake is $\mathrm{d}D = u_{\max}$, where $u_{\max} \approx 5 \times 10^{-5}L$ (Wells and Coppersmith, 1994). Combining these differential equations gives the increase in maximum displacement as a function of the increase in fault length: $\mathrm{d}D/\mathrm{d}L = 5 \times 10^{-5} p_1^{-1} L^{1-p_2}$. Integration then links the maximum displacement and length of the fault at any point on the assumed growth trend:

$$D = \int_{L_{\min}}^{L} 5 \times 10^{-5} p_1^{-1} L^{1-p_2}\, \mathrm{d}L = \frac{5 \times 10^{-5}}{p_1(2-p_2)}\left[L^{2-p_2} - L_{\min}^{2-p_2}\right].$$

If the initial fault size is very small (i.e. $L_{\min}$ is assumed to be zero), this relationship can be equated with the standard form of the displacement/length relationship (i.e. with $D = BL^n$) to give $p_1 = 5 \times 10^{-5}/Bn$ and $p_2 = 2 - n$.

A growth model in which $p_2 = 1$, therefore, gives an increase in fault length per earthquake that is a constant fraction of the length of the fault, and results in a linear trend ($n = 1$) between length and displacement. This is the type of model considered by Peacock and Sanderson (1996). If $p_2 = 0$ the fault will increase in length by a constant amount irrespective

of its size. This results in a growth profile with $n = 2$, equivalent to the growth model considered by Walsh and Watterson (1987). In Fig. 7 we examine displacement profiles for faults grown according to the power-law growth function for two cases each at $n = 1.0$, 1.5 and 2.0 which straddle measured displacement/length data (Fig. 7a). In the models the faults grow from an initial zero-displacement, 1 mm long flaw through repeated micro- then macro-earthquakes with elliptical slip profiles. The shape (Δ) of the resultant displacement profiles for models containing Characteristic earthquakes is shown in Fig. 7b, as a function of the length of the growing fault. Larger faults ($L > 2000$ m) have displacement profiles that depend only on exponent n. Bell-shaped displacement profiles with $\Delta = 0.524$ are obtained when $n = 2.0$, but for the more generally accepted value of $n = 1.0$, faults have unrealistic (compared to natural faults) pointed displacement profiles ($\Delta = 0.393$). These stable displacement profiles are shown in Fig. 7c, and are identical to those obtained by Gillespie et al. (1992). Smaller faults have higher shape factors sensitive to B, with the greatest dependence when $n = 2.0$ (Fig. 7b). This is because the convergence of the profile is related to the number of earthquakes (Peacock and Sanderson, 1996) which, for the same length of the fault, is smaller for higher values of n.

The power-law growth function can also be used to determine the shapes of propagating faults growing with Gutenberg–Richter, rather than Characteristic, earthquakes. In this case the propagation function $dL = p_1 L^{p_2}$ is taken as the increase in fault length per G–R cycle, and the shape of the slip profile aggregated over each G–R cycle depends on the magnitude range of earthquakes contained in the cycle (e.g. Fig. 5b for elliptical slip profiles). Fig. 7d shows the shape factors of propagating faults with different values of n, as a function of earthquake magnitude range. Like the constant length faults (Fig. 5), these profiles become stable for magnitude ranges greater than ca. 2 (Fig. 7d), but unlike them are all distinctly pointed, with stable shape factors ranging from $\Delta = 0.410$ if $n = 2.0$ to $\Delta = 0.309$ if $n = 1.0$ (Fig. 7c).

These results demonstrate incompatibility between elliptical slip profiles, triangular displacement profiles and a propagating fault growth model. For the generally preferred value of $n = 1.0$, the incompatibility is present irrespective of whether

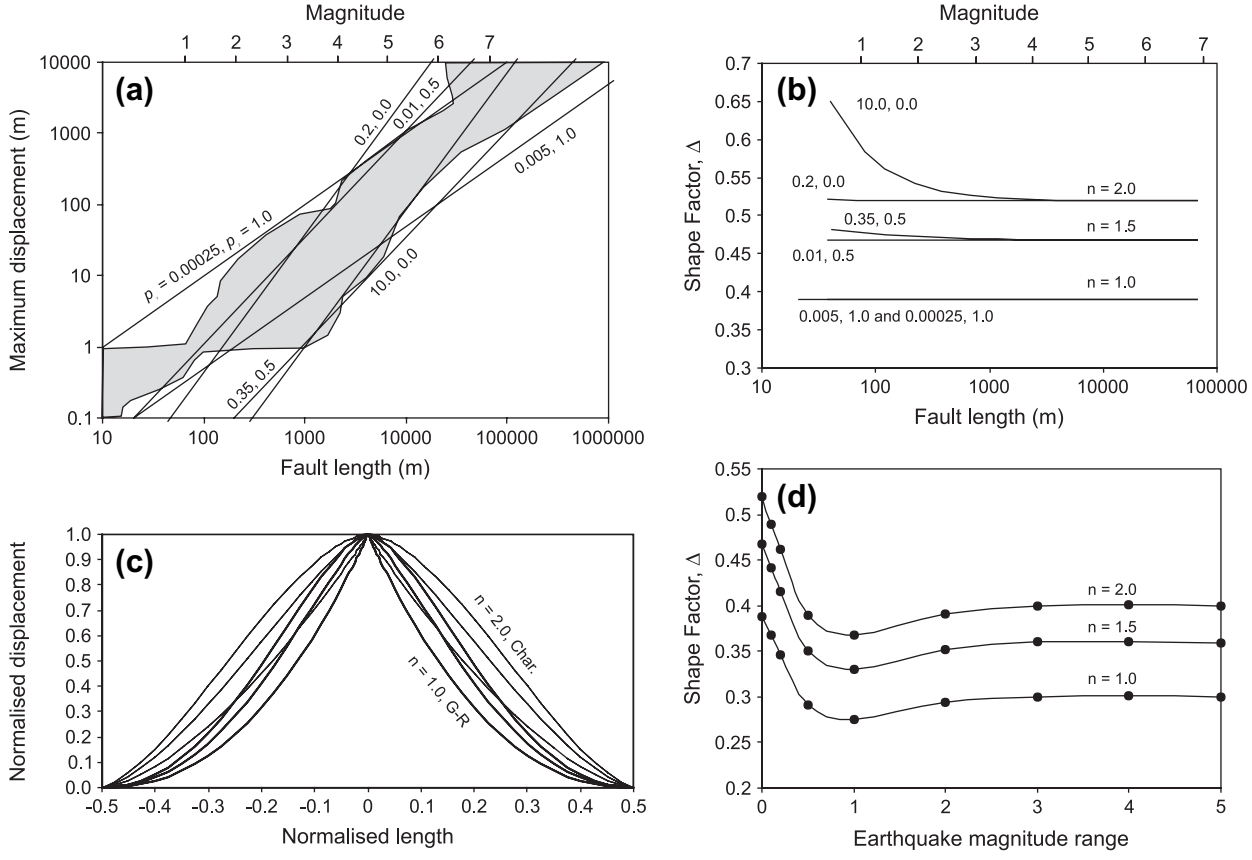

Fig. 7. (a) Maximum fault displacement vs. fault length showing different assumed growth curves for propagating faults. The values of p_1 and p_2 defining the growth are labelled on each curve (see text for discussion). The shaded area outlines the region of measured faults (Schlische et al., 1996). The maximum magnitudes of earthquakes for faults of different lengths are indicated on top of the diagram; these are calculated from the empirical ratio between maximum co-seismic slip and fault length of 5×10^{-5} (Wells and Coppersmith, 1994). (b) Fault displacement shape factor (Δ) vs. fault length for the six growth curves shown in (a), assuming Characteristic earthquakes. (c) Normalised displacement profiles for faults capable of sustaining an M7 earthquake assuming propagating fault growth models with $n = 1$ (lower curves), 1.5 and 2.0 (upper curves) for Characteristic (thinner lines) and G–R (thicker lines) earthquake populations. (d) Fault displacement shape factor vs. the magnitude range of earthquakes in a G–R population, for large faults with propagating fault growth models and different values of n. All model results in (b–d) assume elliptical slip profiles.

the faults grow through Characteristic or G–R earthquakes. By contrast, we have shown in previous sections that the growth model consistent with available fault growth histories, in which faults accumulate most of their displacement with no increase in fault length, results in near-triangular displacement profiles from elliptical slip profiles provided the earthquakes have a magnitude range in excess of 0.5.

5. Discussion and conclusions

Our modelling suggests that the near-triangular displacement profiles associated with non-interacting faults are compatible with a Gutenberg–Richter population of earthquakes with elliptical slip profiles for a fault growth model in which fault length is established early, and for the bulk of the growth history the fault accumulated displacement with little or no change in length (i.e. the growth model of Walsh et al., 2002). These ideal fault displacement and earthquake slip profiles are incompatible with the generally accepted fault growth history in which displacement accumulates in proportion to increasing fault length, irrespective of the earthquake population.

A requirement for the development of realistic displacement profiles on non-propagating faults is that the earthquake magnitudes must range over at least half a magnitude unit. Although by strict definition this implies that realistic displacement profiles cannot emerge on non-propagating faults through Characteristic earthquakes, in practice an earthquake population ranging in magnitude over half a unit below the maximum present is much more likely to be interpreted as Characteristic than Gutenberg–Richter (e.g. Wesnousky, 1994). Triangular displacement profiles, however, are perhaps most complementary with a weakly Characteristic earthquake model (Hamilton and McCloskey, 1997; Steacy and McCloskey, 1999) comprising a G–R earthquake population with an anomalously high frequency of maximum-magnitude events. Our measure of fault shape (Δ, the average displacement normalised by the maximum displacement) is a first order approximation taking no account of the presence of inflection points in the profile. Despite having $\Delta > 0.5$, all displacement profiles generated from elliptical slip distributions on non-propagating faults have an inflection point, with the tip displacement gradients approaching (but never equalling) zero (Fig. 5b). A displacement profile arising from strictly Characteristic earthquakes with elliptical profiles, however, has no inflection point and a maximum slip gradient at the fault tip. Combining these two types of normalised displacement profiles in a proportion commensurate with a weakly Characteristic earthquake population therefore results in displacement profiles with constant tip gradients. This observation contrasts with the results from propagating fault growth models which universally produce tip gradients tending to zero (Fig. 7c) irrespective of whether the earthquake size distribution is Characteristic, weakly Characteristic or Gutenberg–Richter.

One of the principal differences between our model for displacement accumulation and certain earlier models (e.g., Cowie and Scholz, 1992) is that elastic strains are not accumulated during fault growth. If elastic strains were to accumulate then displacement profiles should continuously readjust to provide, ideally, semi-elliptical profiles. To circumvent this problem previous fault growth models envisaged that (i) slip-related elastic strains were relaxed rapidly (i.e. on earthquake cycle time scales; Walsh and Watterson, 1987, 1988), with individual earthquakes accompanied by fault propagation and associated inelastic deformation, (ii) displacement profiles are elastic over much of the fault surface with inelastic deformation associated with fault propagation within a fault process zone (Cowie and Scholz, 1992), or (iii) displacement profiles are elastic with displacement loss and linear displacement profiles arising from the existence of fault damage zones extending into the rock volume surrounding the fault (Manighetti et al., 2001, 2004). Our model is, in that respect, very reminiscent of that of Walsh and Watterson (1987, 1988), in which elastic strains, and associated stresses, are not retained on long time scales but are instead relaxed to permanent strains by a variety of small-scale deformation processes, such as micro-fracturing, compaction and pressure solution. Our modelling shows that for a fault with constant length and in the absence of strong interactions with adjacent faults, elliptical earthquake slip profiles will provide near-triangular displacement profiles. The presence of adjacent strongly interacting faults will lead to changes in displacement profiles, such that adjacent co-linear faults will not only show earthquake clustering behaviour but will also show aggregate displacement profiles that, in the limit, approach the constant displacement condition of interplate faults.

Acknowledgements

This paper is the result of studies completed with financial support from the Royal Society of New Zealand Marsden Fund (GNS 902) and the Enterprise Ireland Basic Research Grant Scheme (SC/00/041). An anonymous reviewer is thanked for constructive criticism.

References

Childs, C., Nicol, A., Walsh, J.J., Watterson, J., 2003. The growth and propagation of synsedimentary faults. Journal of Structural Geology 25, 633–648.

Cladouhos, T.T., Marrett, R., 1996. Are fault growth and linkage models consistent with power-law distributions of fault length? Journal of Structural Geology 18, 281–293.

Cowie, P.A., Scholz, C.H., 1992. Growth of faults by accumulation of seismic slip. Journal of Geophysical Research 97, 11085–11095.

Eshelby, J.D., 1957. The determination of the elastic field of an ellipsoidal inclusion and related problems. Philosophical Transactions of the Royal Society of London A 241, 376–396.

Gillespie, P.A., Walsh, J.J., Watterson, J., 1992. Limitations of dimension and displacement data from single faults and the consequences for data analysis and interpretation. Journal of Structural Geology 14, 1157–1172.

Gutenberg, B., Richter, C.F., 1944. Frequency of earthquakes in California. Bulletin of the Seismological Society of America 34, 185–188.

Hamilton, T., McCloskey, J., 1997. Breakdown of power-law scaling in an analogue model of rupture and stick-slip. Geophysical Research Letters 24, 465–468.

Main, I., 1990. Apparent breaks in scaling in the earthquake cumulative frequency–magnitude distribution: fact or artefact? Bulletin of the Seismological Society of America 90, 86–97.

Manighetti, I., King, G., Gaudemer, Y., Scholz, C., Doubre, C., 2001. Slip accumulation and lateral propagation of active normal faults in Afar. Journal of Geophysical Research 106, 13667–13696.

Manighetti, I., King, G., Sammis, C.G., 2004. The role of off-fault damage in the evolution of normal faults. Earth and Planetary Science Letters 217, 399–408.

McCalpin, J.P., Nelson, A.R., 1996. Introduction to paleoseismology. In: McCalpin, J.P. (Ed.), Paleoseismology. Academic Press, San Diego, California, pp. 1–31.

Meyer, V., Nicol, A., Childs, C., Walsh, J.J., Watterson, J., 2002. Progressive localisation of strain during the evolution of a normal fault system in the Timor Sea. Journal of Structural Geology 24, 1215–1231.

Morewood, N.C., Roberts, G.P., 1999. Lateral propagation of the surface trace of the South Alkyonides normal fault segment, central Greece: its impact on models of fault growth and displacement–length relationships. Journal of Structural Geology 21, 635–652.

Nicol, A., Watterson, J., Walsh, J.J., Childs, C., 1996. The shapes, major axis orientations and displacement patterns of fault surfaces. Journal of Structural Geology 18, 235–248.

Nicol, A., Walsh, J.J., Berryman, K., Nodder, S., 2005. Growth of a normal fault by accumulation of slip over millions of years. Journal of Structural Geology 27, 327–342.

Peacock, D.C.P., Sanderson, D.J., 1996. Effects of propagation rate on displacement variations along faults. Journal of Structural Geology 18, 311–320.

Pollard, D.D., Segall, P., 1987. Theoretical displacements and stresses near fractures in rock: with applications to faults, joints, veins, dikes, and solution surfaces. In: Atkinson, B.K. (Ed.), Fracture Mechanics of Rock. Academic Press, New York, pp. 277–349.

Poulimenos, G., 2000. Scaling properties of normal fault populations in the western Corinth Graben, Greece: implications for fault growth in large strain settings. Journal of Structural Geology 22, 307–322.

Schlishe, R.W., Young, S.S., Ackerman, R.V., Gupta, A., 1996. Geometry and scaling relations of a population of very small rift-related normal faults. Geology 24, 683–686.

Scholz, C.H., 1990. The Mechanics of Earthquakes and Faulting. Cambridge University Press.

Schwartz, D.P., Coppersmith, K.J., 1984. Fault behavior and characteristic earthquakes: examples from the Wasatch and San Andreas fault zones. Journal of Geophysical Research 89, 5681–5698.

Steacy, S., McCloskey, J., 1999. Heterogeneity and the earthquake magnitude–frequency distribution. Geophysical Research Letters 26, 899–902.

Walsh, J.J., Watterson, J., 1987. Distributions of cumulative displacement and seismic slip on a single normal fault surface. Journal of Structural Geology 9, 1039–1046.

Walsh, J.J., Watterson, J., 1988. Analysis of the relationship between the displacements and dimensions of faults. Journal of Structural Geology 10, 239–247.

Walsh, J.J., Nicol, A., Childs, C., 2002. An alternative model for the growth of faults. Journal of Structural Geology 24, 1669–1675.

Wells, D.L., Coppersmith, K.J., 1994. New empirical relationships among magnitude, rupture length, rupture width, rupture area, and surface displacement. Bulletin of the Seismological Society of America 84, 974–1002.

Wesnousky, S.G., 1994. The Gutenberg–Richter distribution or characteristic earthquake distribution: which is it? Bulletin of the Seismological Society of America 84, 1940–1959.